Compact Filtering Power Divider With Sharp Roll-Off Skirt and Deep Suppression Using Coupled Square Ring Resonator

Daotong Li, *Senior Member, IEEE,* Luqi Zhang, Ying Liu, Chen Yang, and Qiang Chen, *Senior Member*

***Abstract*—In this paper, a novel compact filtering power divider (FPD) with sharp frequency selectivity, high in-band isolation and deep out-of-band suppression is proposed. The realization of filtering and power division functions is achieved by utilizing of a U-shaped resonator coupled square ring resonator (UR-CSRR). The UR-CSRR configuration is proposed using a modified U-shaped resonator (UR) coupled with a modified square ring resonator (SRR). By loading a pair of open stubs at the ends and a stepped impedance open stub at the center of an SRR, the modified SRR with two controllable transmission zeros (TZs), which can be used to adjust the bandwidth and improve the upper stopband, is realized. The modified UR is formed by loading a single open stub and two pairs of open stubs with the ability to generate a controllable TZ at the right edge of the passband at the center and in the upper stopband at the ends of a UR, respectively. To generate the output signal, two output lines are inserted on both sides of the single open stub which can also introduce two TZs. In addition, two resistors are introduced between the two output lines to obtain high in-band isolation. To validate this design concept, an FPD with a center frequency of 3 GHz is designed, simulated and measured. Measurements indicate that the minimum in-band insertion loss is 1.1 dB, the 3 dB fractional bandwidth (FBW) is approximately 25%, the out-of-band suppressions of both upper and lower stopband are greater than 30 dB, and the in-band isolation is greater than 25 dB. The simulated and measured results are in good agreement, demonstrating the feasibility of the proposed design strategies.**

***Index Terms*—Coupled lines, deep suppression, filtering power divider, high-selectivity square ring resonator (SRR), U-shaped resonator.**

I. Introduction

IN order to fulfill the necessary requirements for achieving high-performance in radio frequency (RF) components that are compact in size and exhibit many functions, making use of a filtering power divider (FPD) that includes both filtering and power division/combination functions has shown to be an exceedingly successful approach .

Typically, an FPD can be developed by cascading bandpass filters (BPFs) with a power divider (PD) [1], but its circuit size is quite large and the insertion loss is high due to the cascading structure. To solve this problem, FPDs with integrated BPF and PD have been reported recently [2]-[4]. Two pairs of dual resonators are embedded into the output arms of a Wilkinson power divider (WPD), resulting in a dual-band FPD with 3 dB fractional bandwidth (FBW) of 8% and 6%, 18.6 dB in-band isolation and 20 dB upper stopband [2]. An FPD with 12.5% 3 dB FBW and 20 dB stopband rejection level is designed by replacing the λ/4 transmission lines of the WPD with two coupled quasi-lumped resonators [3]. Two coupled substrate integrated defected ground structure resonant cells are cascaded at the arms of the power divider to achieve a filtering response with 3 dB FBW of 23% and 28 dB stopband rejection level [4]. Nevertheless, the bandwidths of the three previously mentioned FPDs are limited, which also necessitates an enhancement in frequency selectivity. Extensive investigations have been conducted to examine the attributes of wide passband along with excellent frequency selectivity. [5]-[11]. For example, an FPD with 3 dB FBW of 63.6% and sharp roll-off skirts is proposed by using a simple structure composed of a coupled-line terminal loading quad-mode resonator and stepped-impedance resonator [5]. A bandpass WPD with 3 dB FBW of 66% consisting of coupled line sections, short-circuited stubs and isolation resistors is proposed in [9]. Despite achieving wideband characteristics, the in-band isolation is limited to a maximum of -18 dB. To address this issue, previous studies have documented the development of FPDs with higher in-band isolation capabilities [11] - [13]. An FPD with 3 dB FBW of 19.6% and -20 dB isolation is proposed by adopting doubly-stub-loaded parallel-coupled lines, T-shaped stub, short-circuited and open-circuited branches [11]. But it has no more than -20dB upper stopband rejection level. By embedding a pair of multimode resonators and three isolated resistors, an FPD with 47.6% 3 dB FBW and -20.2dB in-band isolation is proposed [13]. However, it suffers from poor frequency selectivity and input/output return loss. There is an urgent demand for research on how to build FPDs with wideband, sharp

This work was supported in part by the National Natural Science Foundation of China under Grant 61801059, in part by the FY2021 JSPS Postdoctoral Fellowship for Research in Japan under Grant P21053, and in part by the Grant-in-Aid for JSPS Research Fellow under Grant 21F21053, in part by the Opening Fund of State Key Laboratory of Millimeter Waves under Grant K202016, in part by the Basic Research and Frontier Exploration Special of Chongqing Natural Science Foundation under Grant cstc2019jcyj-msxmX0350.

Daotong Li, Luqi Zhang, Ying Liu, Chen Yang and are with School of Microelectronics and Communication Engineering, Chongqing University, Chongqing 400044, China (e-mail: dli@cqu.edu.cn).

Daotong Li and Qiang Chen are with the Department of Communications Engineering, Tohoku University, Sendai 980-8579, Japan (e-mail: qiang.chen.a5@tohoku.ac.jp).

selectivity, excellent in-band isolation and deep out-of-band suppression. It is worth noting that most of the above mentioned FPD designs are limited to the topology based on two-way double resonators to achieve functions of filtering and power division/combination at the same time, which always results in a relatively large size and complex design. For example, the size of the FPD using two-way double resonators in [10] is 1.54 λ_g ×0.56λ_g. Despite the tiny dimensions of 0.46λ_g×0.23λ_g [4] and 0.38λ_g×0.25λ_g [11] of FPDs, these devices employ multilayers to achieve size reduction. However, this approach also introduces additional complexity and cost to the design. To the best of our knowledge, there are few reports on the design of microstrip FPDs based on only a resonator and a single layer.

This paper aims to present a novel and simple integrated design to show an FPD with sharp roll-off skirts, deep out-of-band suppression and high in-band isolation. This FPD is designed by using a U-shaped resonator coupled square ring resonator (UR-CSRR) and two resistors. The bandpass response is obtained by using a UR-CSRR which is proposed by a modified U-shaped resonator (UR) coupled with a modified square ring resonator (SRR). The modified SRR consists of a pair of open stubs loaded at the ends, and a step impedance open stub placed in the center of the SRR. The modified UR is achieved by implementing two pairs of open stubs and a single open stub positioned at the ends and center of the UR, respectively. Two output lines are introduced between both sides of the single open stub loaded on the UR. In addition, two resistors are used between the two output lines to achieve high in-band isolation. With the three pairs of open stubs and the stepped impedance open stub loaded on the UR-CSRR, six transmission zeros (TZs) are generated to improve the roll-off skirt of passband and the upper stopband rejection level. In general, the proposed novel design method of FPD has the advantages of (1) wideband and excellent frequency selectivity, (2) controllable TZs and deep and wide out-of-band suppression, (3) simple and compact structure.

To explain the working mechanism of the circuit, the theoretical analysis and deduction of the U-shaped resonator coupled SRR and the proposed FPD are presented in Section II. To validate the theoretical derivation, Section III provides the characteristics, simulated and measured results of the proposed FPD. In section IV, a conclusion is provided.

II. Theoretical Analysis of Proposed FPD

A. Configuration of the Proposed FPD

The circuit structure of the proposed FPD, which consists of a UR-CSRR, two resistors (R_1 and R_2), one input port (Port 1), and two output ports (Port 2 and Port 3), is depicted in Fig. 1. It can be seen that the UR-CSRR (in red dashed box) is proposed by a modified UR (in green box) coupled with a modified SRR (in blue box). The modified SRR is formed by a pair of open stubs (Z_2, θ_s=θ_{c2}+θ_{s1}) loaded at the ends and a step impedance open stub (Z_3, Z_4 and θ_{s2}=θ_3+θ_4) loaded at the center of a SRR (Z_2, θ_{SRR}=2(θ_2+θ_{c1})). The modified UR is formed by using a UR (Z_5, 2θ_c=θ_{c1}+θ_{c2} and Z_6, 2θ_6) loaded with two pairs of open stubs (Z_7, θ_{s3} and Z_6, θ_{s4}) at the ends and an open stub (Z_t, θ_t) at the middle. To ensure that two output signals exhibit the same amplitude and in-phase property, two output lines are symmetrically placed on opposite sides of the open stub of the modified UR. Meanwhile, resistors are mounted between the two output lines to improve the in-band port isolation.

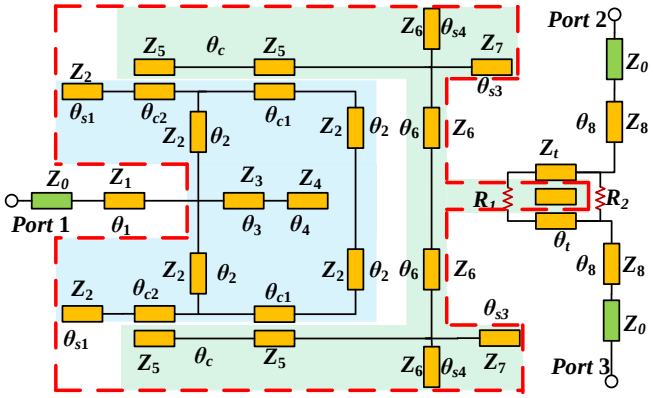

Fig.1. Schematic of the proposed FPD.

B. Analysis and Design of the Proposed FPD

The designed layout of the proposed FPD is described in Fig.2. The signal is initially input at Port 1, propagated through the UR-CSRR structure, and then equally divided and coupled to the two output lines at Port 2 and Port 3. A detailed study of the UR-CSRR is carried out to clarify the characteristics of the proposed FPD.

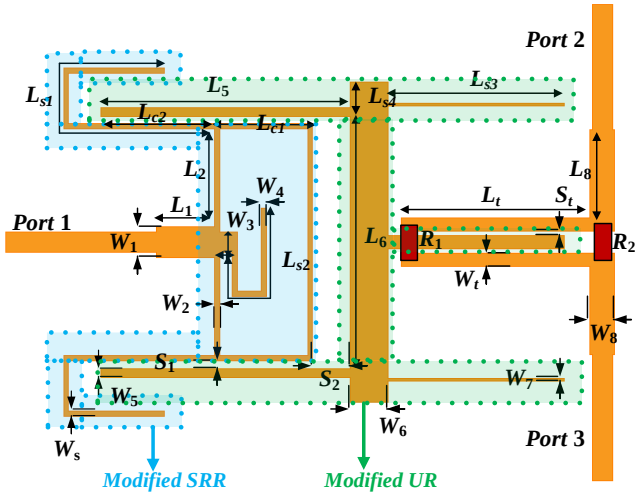

Fig.2. Layout of the proposed FPD.

As shown in Fig.3 (a), the UR-CSRR is symmetric with its central plane, so the odd- and even-mode analysis methods can be utilized to analyze its resonance property. Fig.3 (b) and (c) depict the equivalent even-mode and odd-mode circuit models, respectively.

To facilitate the calculation of its characteristics, it is assumed that the impedance of each transmission line segment is Z_0. From the lossless transmission line theory, the input impedance of the even-/odd-mode equivalent circuits, can be written as

$$Z_{ine} = \frac{-jZ_0 Z_{ine1}\cos\theta_{s2}}{Z_{ine1} - jZ_0\cos\theta_{s2}} \tag{1}$$

$$Z_{ino} = \frac{jZ_0 Z_{ino1}(\tan\theta_2 - \tan\theta_s) + Z_0^2\tan\theta_2\tan\theta_s}{Z_{ino1} - jZ_0\tan\theta_s} \tag{2}$$

where,

$$Z_{ine1} = \frac{-jZ_0 Z_{ine2}(\tan\theta_2 + \tan\theta_s) + Z_0^2\tan\theta_2\tan\theta_s}{jZ_0\tan\theta_s - Z_{ine2}} \tag{3}$$

$$Z_{ine2} = \frac{-j(Z_e+Z_o)\cot\theta_c}{2} - \frac{-j(Z_e+Z_o)\csc^2\theta_c\tan\theta_2}{2Z_0 - (Z_e+Z_o)\cot\theta_c\tan\theta_2} + Z_{ine3} \tag{4}$$

$$Z_{ine3} = -jZ_0\frac{\tan\theta_{s3}\tan\theta_{s4}\tan(\theta_t+\theta_6)}{\tan(\theta_0+\theta_6)(\tan\theta_{s3}+\tan\theta_{s4}) + \tan\theta_{s3}\tan\theta_{s4}} \tag{5}$$

$$Z_{ino1} = \frac{-j(Z_e+Z_o)\cot\theta_c}{2} + \frac{-(Z_e+Z_o)\cot\theta_c\cot\theta_2}{2Z_0 + (Z_e+Z_o)\cot\theta_c\cot\theta_2} + Z_{ino2} \tag{6}$$

$$Z_{ino2} = -jZ_0\frac{\tan\theta_{s3}\tan\theta_{s4}\tan\theta_6}{\tan\theta_6(\tan\theta_{s3}+\tan\theta_{s4}) - \tan\theta_{s3}\tan\theta_{s4}} \tag{7}$$

Z_e and Z_o are the even and odd mode impedance of the parallel coupled of the UR-CSRR.

When Z_{ine}=∞ and Z_{ino}=∞, two resonant frequencies can be derived:

$$f_1 = \frac{2f_0}{\pi}\operatorname{arccot}\frac{-Z_0}{Z_a\cot\theta_2} \tag{8}$$

$$f_2 = \frac{2f_0}{\pi}\operatorname{arccot}\frac{Z_0\tan\theta_2\tan\theta_{s2}\cot\theta_c}{Z_a^2\csc^2\theta_c + \tan(\theta_6+\theta_t)} \tag{9}$$

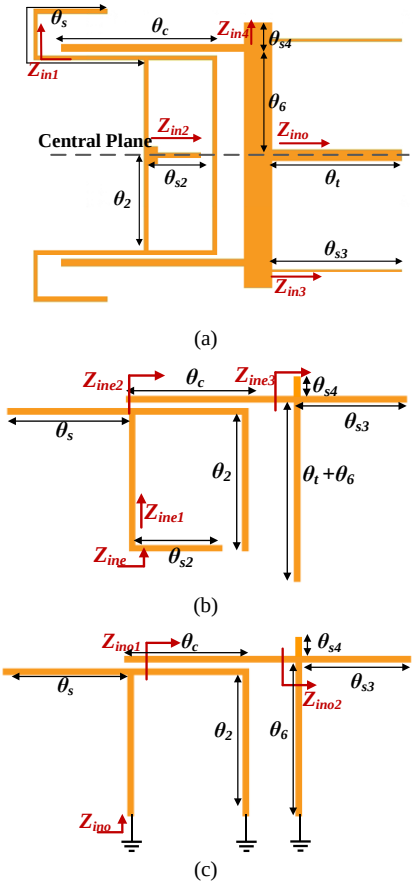

Fig.3. (a) Configuration of the proposed UR-CSRR. (b) Equivalent circuit model of even-mode bisection. (c) Equivalent circuit model of odd-mode bisection.

Moreover, when the input impedances of Z_{in1}=Z_{in2}=Z_{in3}= Z_{in4}= 0, current in the circuit will be directly shorted to ground and four controllable TZs can be introduced. And the locations of the TZs can be written as:

$$f_{TZ2n} = \frac{(2n-1)\cdot 90^o}{\theta_s} f_0 (n = 1, 2...) \tag{10}$$

$$f_{TZ3n} = \frac{(2n-1)\cdot 90^o}{\theta_{s3}} f_0 (n = 1, 2...) \tag{11}$$

$$f_{TZ4n} = \frac{(2n-1)\cdot 90^o}{\theta_{s2}} f_0 (n = 1, 2...) \tag{12}$$

$$f_{TZ6n} = \frac{(2n-1)\cdot 90^o}{\theta_{s4}} f_0 (n = 1, 2...) \tag{13}$$

Furthermore, the external *Q*-factor can be described by:

$$Q_e = \frac{1}{FBW\cdot m_{su}^2} \tag{14}$$

where FBW and m_{su} represent the 3 dB fractional bandwidth and the normalized coefficient between the modified SRR and the modified UR, respectively.

The coupling coefficient between the modified SRR and the modified UR is given by:

$$k_{su} = \frac{f_{02}^2 - f_{01}^2}{f_{02}^2 + f_{01}^2} \tag{15}$$

where f_{01} and f_{02} stand for the lower and higher resonant frequencies of the UR-CSRR.

The relationship between k_{su} and m_{su} can be converted through:

$$k_{us} = FBW\cdot m_{su} \tag{16}$$

For the proposed FPD, similarly, the odd- and even-mode analysis methods can be adopted due to the symmetrical structure. The even- and odd-mode equivalent circuits of the proposed FPD are depicted in Fig.4 (a) and (b), respectively. For the parallel coupled output line section, two TZs can be generated when its input impedance equal to zero:

$$f_{TZ1} = 0 \tag{17}$$

$$f_{TZ5} = \frac{2f_0}{\pi}\arccos\frac{(Z_{oe}-Z_{oo})^2}{(Z_{oe}+Z_{oo})^2} \tag{18}$$

where Z_{oe} and Z_{oo} are the even and odd mode of the parallel coupled output lines, respectively.

Based on the theoretical analysis of the microwave network, the scattering parameters S_{11}, S_{21}, S_{22} and S_{23} can be expressed as follows:

$$S_{11} = \frac{S_{11}^e + S_{22}^e}{2} \tag{19}$$

$$S_{12} = S_{21} = S_{31} = \frac{S_{11}^e - S_{22}^e}{2} \tag{20}$$

$$S_{22} = \frac{S_{22}^e + S_{22}^o}{2} \tag{21}$$

$$S_{23} = \frac{S_{22}^e - S_{22}^o}{2} \tag{22}$$

where S_{11}^e and S_{22}^e respectively represent the input and output

return loss of the even-mode equivalent circuit, and S_{22}^{o} represents the output return loss of the odd-mode equivalent circuit of the proposed FPD.

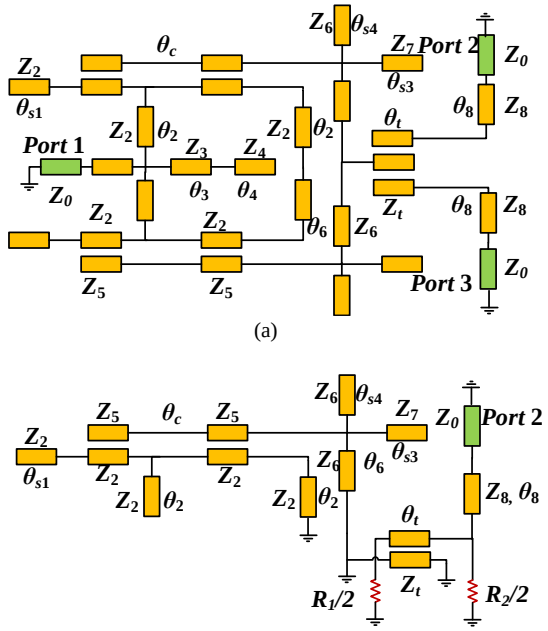

Fig.4 (a)Even-mode and (b) odd-mode equivalent circuits of the proposed FPD.

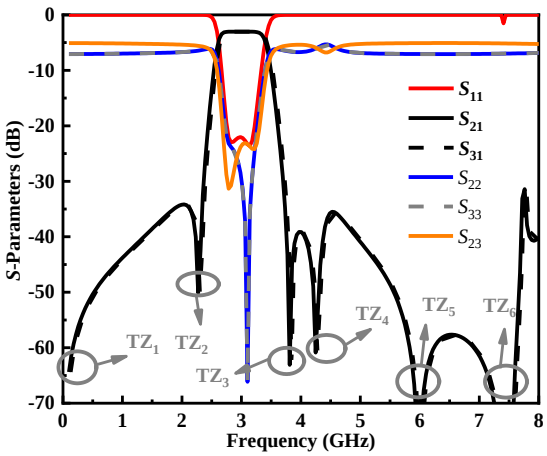

Fig. 5. Calculated results of S_{11}, S_{21} S_{31}, S_{22}, S_{33} and S_{23} on proposed FPD.

TABLE I

CALCULATED PARAMETERS OF PROPOSED FPD

(Substrate: ε_r=2.2, h=0.508mm and tanδ=0.0009)

θ_t	90°	θ_2	45°	θ_c	90°
θ_s	75°	θ_{s2}	65°	θ_{s3}	65°
θ_{s4}	10°	R_1	100Ω	R_2	300Ω

Here, a prototype FPD with a center frequency of f_0=3 GHz and a 3 dB fractional bandwidth (FBW) of 25.4%, as shown in Fig.1, is designed on Rogers 5880 substrate with a relative dielectric constant of 2.2, a thickness of 0.508 mm and a loss tangent of 0.0009. The calculated parameters and responses are shown in TABLE I and Fig.5, respectively. It can be seen from Fig.5 that a total of six TZs and two in-band resonant frequencies are generated, which are consistent with the above analysis.

In order to better understand the working mechanism of the proposed FPD, a numerical analysis is performed to investigate the effects of several key parameters on its performance.

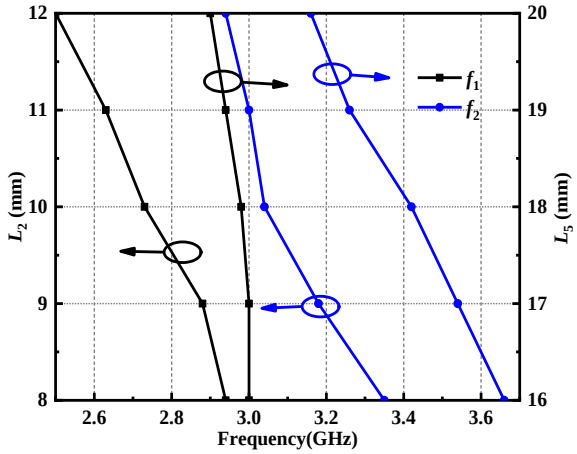

Fig.6. Resonant frequencies versus different L_2 and L_5. (Unit: mm)

Fig. 6 illustrates the resonant frequencies versus different L_2 and L_5. As shown in Fig. 6, when the length L_2 is increased from 8 mm to 12 mm, the first and second resonant frequencies vary in the same direction, moving from 2.94 GHz to 2.45 GHz and from 3.35 GHz to 2.88 GHz, respectively. The second resonant frequency exhibits an apparent decrease from 3.66 GHz to 3.16 GHz as the length of L_5 increases from 16 mm to 20 mm. Therefore, the resonant frequencies can be changed by manipulating of the lengths of SRR and UR, which allows both the center frequency and the bandwidth to be changed.

Fig. 7 (a) and (b) illustrate the frequency responses of the simulated $|S_{21}|$ with different L_{S1} and L_{S3}, respectively. As can be seen from Fig.7 (a), the location of TZ_2 decreases from 2.5 GHz to 2.1 GHz and 3 dB FBW increases from 19.1% to 27% when the value of Ls_1 increases from 14 mm to 18 mm. As shown in Fig. 7 (b), the location of TZ_3 decreases from 4.5 GHz to 3.6 GHz when the value of Ls_3 increases from 11 mm to 15 mm. As TZ_3 moves towards low frequencies, the right edge of the passband becomes steeper. Thus, the passband bandwidth and frequency selectivity of the FPD can be easily controlled by adjusting the lengths of Ls_1 and Ls_3.

Fig. 8 shows the locations of TZ_4 and TZ_6 with different Ls_2 (L_{s2}=L_3+L_4) and L_{s4}, respectively. Fig. 8 illustrates that the locations of TZ_4 move towards from 5.2 GHz to 3.9 GHz when the value of L_{s2} increases from 11 mm to 15 mm. Similarly, as can be seen, the frequencies of TZ_6 move towards lower frequencies from 7.7 GHz to 6.9 GHz as Ls_4 increase from 2 mm to 6 mm. Therefore, the TZ_4 and TZ_6 which are located in the upper stopband are easy to control

individually, and it is possible to take advantage of them to enhance the upper stopband rejection level.

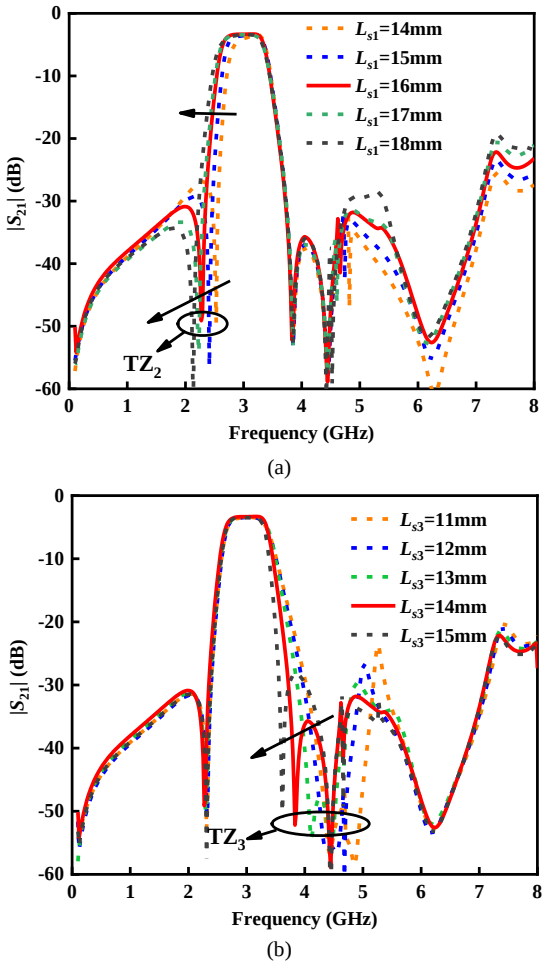

Fig.7 Frequency responses of the simulated $|S_{21}|$ with different (a) L_{S1} and (b) L_{S3}

Fig. 9 (a) shows the extracted external Q_e and out-of-band rejection with different gap S_1 of the proposed UR-CSRR. It can be seen that the extracted external Q_e of the proposed FPD increases from 3.7 to 30.9 and out-of-band rejection decreases from -22 dB to -30 dB by tuning the gap S_1 from 0.1mm to 0.4 mm, under the condition of W_5=0.4 mm. As L_5 increases from 14 mm to 20 mm, Q_e decreases from 65 to 15, under the condition of S_1=0.3 mm. From this, it can be seen that S_1 and L_5 have exactly opposite effects on Q_e. Therefore, by adjusting the out-of-band suppression through S_1 and then adjusting Q_e through L_5, better filtering performance can be achieved. Fig. 9 (b) depicts the coupling coefficient k and 3dB FBW with the width W_t and gap S_t of output lines. Under the condition of S_t=0.1 mm, the coupling coefficient k decreases from 0.45 to 0.31 and FBW increases from 13.4% to 25.4% when W_t increases from 0.2 mm to 1 mm. As the gap S_t increases from 0.1 mm to 0.5 mm, the coupling coefficient k and 3dB FBW decrease from 0.31 to 0.14 and 25.4% to 24.2%, respectively, under the condition of W_t=1 mm. Therefore, the FBW is easier to control by adjusting the width W_t.

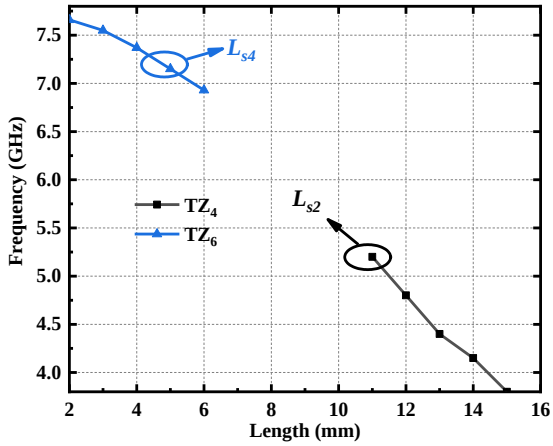

Fig. 8 Locations of TZ_4 and TZ_6 with different L_{s2} and L_{s4}(Unit: mm)

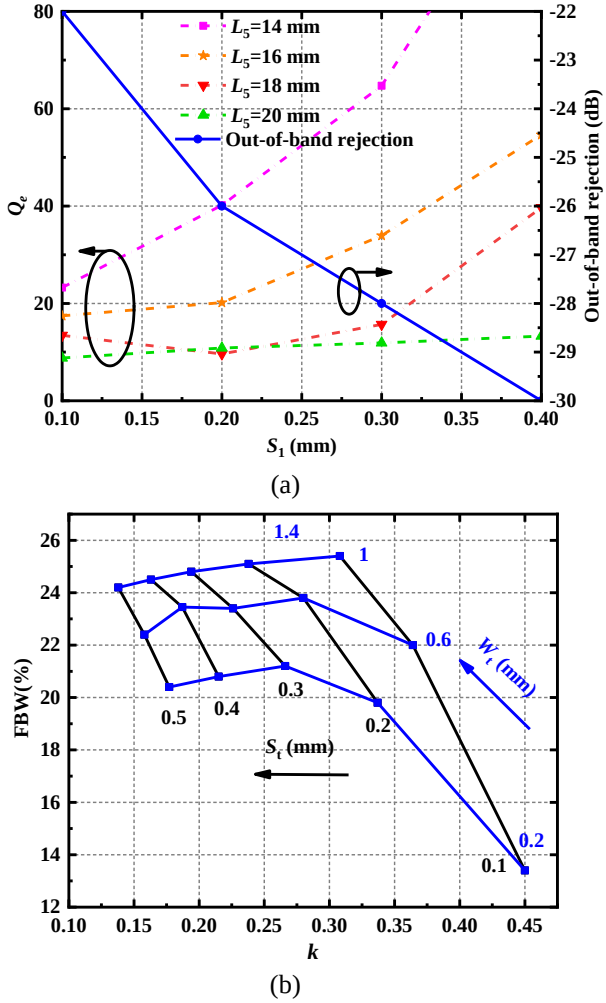

Fig. 9 (a) Extracted external Q_e with varies S_1 and L_5 and out-of-band rejection with varies S_1 (b) coupling coefficient k and 3 dB FBW with varies W_t and S_t

According to Equation (22), isolation is related to both S_{22}^e and S_{22}^o, and it is higher when S_{22}^e and S_{22}^o are closer. Since the even-mode equivalent circuit has been determined, S_{22}^o is designed by adjusting the two resistors in Fig. 1 to be as close to -20 dB as possible to achieve high in-band isolation. Fig. 10(a) shows the odd-mode reflection coefficient S_{22}^o varies

with different R_1 and R_2. As seen in Fig .10 (a), the S_{22}^o is approximately -20 dB when R_1 is 100 Ω and R_2 ranges from 200 to 500 Ω. The magnitudes of S_{23} and S_{22} varied with different R_2 are shown in Fig. 10 (b) and (c), respectively. It can be seen from Fig.10 (b) that the in-band isolation is better than -30 dB when R_2 ranges from 200 to 300 Ω. Fig. 10 (c) shows the magnitude of S_{22} varying with different R_2, the S_{22} is minimum when the value of R_2 is 300 Ω. Finally, the resistance values are determined to be R_1=100 Ω and R_2=300 Ω, where both the simulated S_{23} and S_{22} are less than -32 dB.

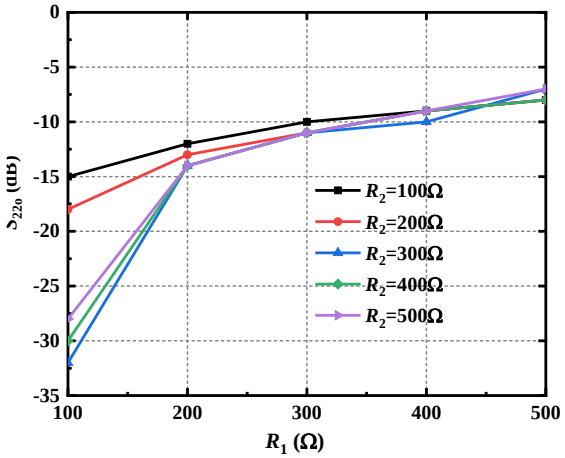

(a)

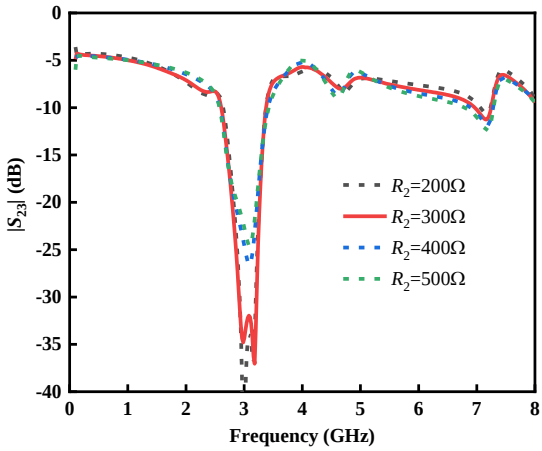

(b)

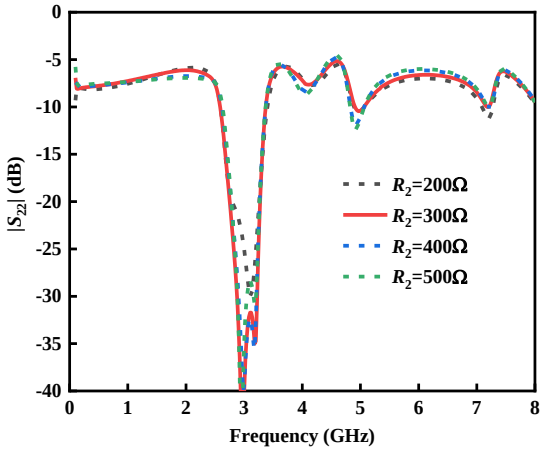

(c)

Fig. 10 The odd-mode reflection coefficient S_{22}^o with varied R_1 and R_2. (b) Magnitude of S_{23} with varied R_2 when R_1 = 100 Ω (c) Magnitude of S_{22} with varied R_2 when R_1 = 100 Ω

According to the theoretical analysis above, the design procedures of the proposed FPD can be summarized as follows:

1) First, according to the required specifications, the required parameters, such as center frequency(f_0), -3 dB FBW, frequency selectivity, out-of-band rejection and return loss in the passband, can be determined.
2) Then, based on the required f_0=3 GHz, the electrical lengths of θ_2=45° and θ_c=90° are determined by equations (8) and (9).
3) Based on the required frequency selectivity and out-of-band suppression, the positions of TZ_2, TZ_3, TZ_4 and TZ_6 are determined by the lengths of three open stubs (θ_s=75°, θ_{s2}=65°, θ_{s3}=65°, θ_{s4}=10°) according to equations (10) to (13).
4) Assuming equal propagation constants, the impedance coefficient at specific physical parameters (W_t=0.9mm and S_t=0.1mm) can be approximated by extracting the *Z*-matrix parameter curve from the physical model and selecting the Z-parameter value at half the frequency corresponding to θ_t = 90°.
5) For the required in-band isolation and output return loss, the value of R_1=100 Ω, R_2=300 Ω can be calculated form equation (22) and selected from Fig. 10.
6) Finally, after the initial designed sizes are obtained, fine-tune the other parameters by using the full-wave EM simulation software for a minimum insertion loss and a good input match over the design passband.

III. Implementation and Results

To validate the design procedure, an FPD with a center frequency of 3 GHz is designed, simulated, fabricated, and measured. The design parameters of the FPD are shown in TABLE II, and the selected resistors are R_1=100 Ω and R_2=300 Ω. The effective circuit area of the proposed FPD is $0.41\lambda_g \times 0.65\lambda_g$, where λ_g is the waveguide wavelength at the center frequency.

TABLE II
FABRICATED PARAMETERS OF PROPOSED FPDS (unit: mm)
(Substrate: ε_r=2.2, h=0.508mm and $\tan\delta$ = 0.0009)

W_1	2	W_2	0.4	W_3	1.6	W_4	0.4	W_5	0.7
W_6	3	W_t	0.9	W_{s1}	0.4	W_{s2}	0.2	W_8	2
L_1	4.6	L_2	9	L_3	1	L_4	13.2	L_5	19.8
L_6	25	L_t	14	L_{s1}	15.8	L_{s2}	14	L_8	7
S_1	0.4	S_2	S_t	0.1					

TABLE III

COMPARISON OF PROPOSED WORK WITH REPORTED ONES

Refs.	f_0/FBW (GHz/%)	IL (dB)	RL (dB)	ISO (dB)	OBR (dB)	SF	Technology
[4]	2.87/23	1	15	20	28	3.18	3 layers/SIDGS
[7]	2.2/48.2	0.55	14	10	30	2.36	1 layer/Microstrip
[10]	3/26	N.A.	23.1	21.6	15.3	2.18	1 layer/Microstrip
[11]	2.45/19.6	0.59	15	20	19.5	1.35	2 layers/Microstrip
[15]	4.82/11.6	2	13	N.A.	25	1.88	1 layer/HMSIW
[16]	3.4/17.6	1.4	14	22	20	1.5	2 layers/Microstrip
[17]	5.99/25	1.05	20	21	20	2	1 layer/SIW
This work	**3/25**	**1.1**	**25**	**25**	**30**	**1.68**	**1 layer/Microstrip**

Refs.: References; FBW: 3 dB fractional bandwidth; IL: Insertion Loss; RL: Return Loss; ISO: In-band isolation; OBR: Out-of-band rejection; SF: Shape factor SF = $(f_2^{25dB}\text{-}f_1^{25dB})$ / $(f_2^{3dB}\text{-}f_1^{3dB})$.

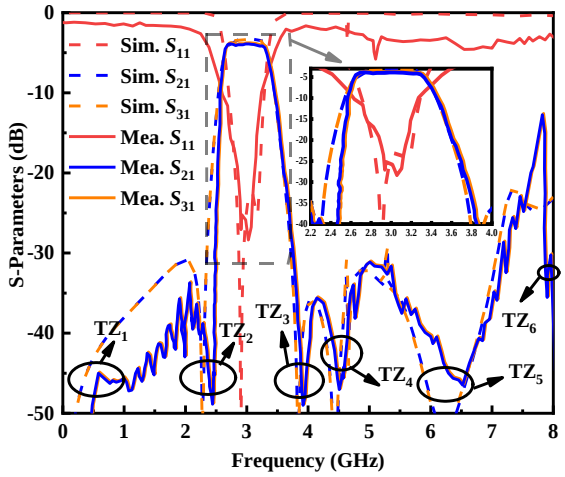

(a)

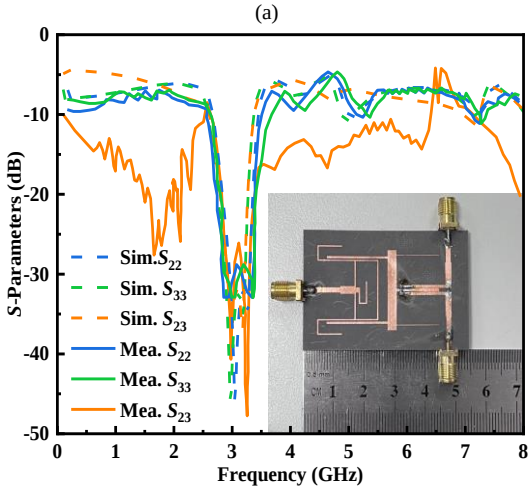

(b)

Fig. 11. Comparison of measured and simulated results of (a) S_{11}, S_{21} and S_{31}. (b)S_{22}, S_{33} and S_{23}.

Fig. 11 depicts the measured and simulated results of the proposed FPD. It can be seen from Fig. 11 (a) that the FPD is centered at 3 GHz with a 3 dB FBW of 25% ranging from2.61 GHz to 3.36 GHz. The in-band insertion loss and return loss are 1.1 dB and 25 dB, respectively. The measured results show that the six TZs are located at 0 GHz, 2.4 GHz, 3.9 GHz, 4.4 GHz, 6.5 GHz and 8GHz, respectively, resulting in out-of-band rejections better than 30 dB and a very sharp frequency selectivety of 1.68. Fig. 11 (b) shows that the in-band isolation is better than 25 dB, and the responses of S_{22} and S_{33} are 27 dB. The simulated and measured results are in good agreement. Fig. 12 shows the magnitude and phase differences between the two output ports, where the in-band amplitude imbalance

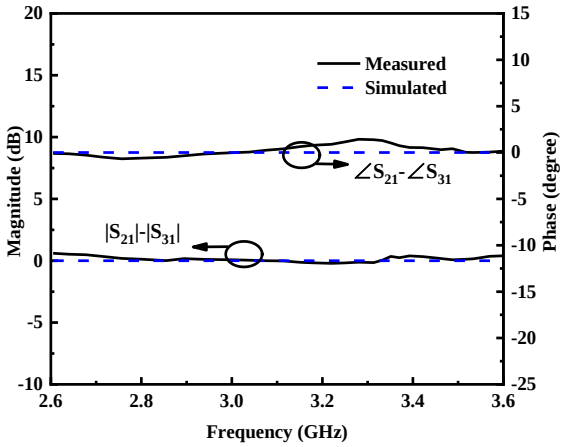

Fig. 12. Simulated and measured magnitude and phase difference between two output ports.

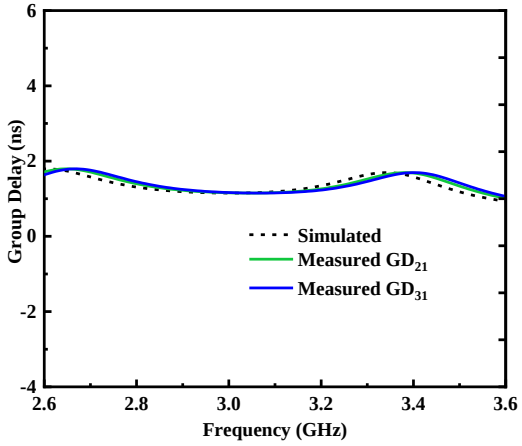

Fig.13 Simulated and measured group delay

is less than ± 0.6dB, and the phase difference within the passband is less than ± 1.5°. Fig. 13 depicts both simulated and measured group delay, which is relatively flat in the passband.

To highlight the advantages of our proposed work, TABLE III provides a summary of the comparison of the proposed FPD in this work and the recently reported counterparts. It can be concluded that our design shows the advantages of sharp frequency selectivity, high out-of-band rejection, and high in-band isolation simultaneously.

IV. Conclusion

In this paper, a compact microstrip FPD based on a UR-CSRR and two resistors is presented. The implementation of filtering and power division functions is achieved by using a single UR-CSRR in a single layer. The UR-CSRR, which consists of a modified UR and a modified SRR, generates two inherent TZs and four adjustable TZs to improve frequency selectivity and out-of-band rejection. The analysis and design procedures are described. To verify the effectiveness of the design concept, an FPD with center frequency at 3 GHz is fabricated and measured. The experimental results indicate that the proposed FPD with 3 dB FBW of 25% exhibits high in-band isolation of no less than 25 dB, sharp bandpass selectivity, and out-of-band rejection level of no less than 30 dB. With these distinctive features, the proposed filtering power divider has a promising application in high sensitivity integrated RF front-end modules.

References

[1] S. W. Wong and L. Zhu, "Ultra-wideband power divider with good in-band splitting and isolation performances," *IEEE Microwave and Wireless Components Letters*, vol. 18, no. 8, pp. 518–520, Aug. 2008.

[2] P. Wen, "Dual-Band Filtering Power Divider Using Dual-Resonance Resonators With Ultrawide Stopband and Good Isolation," *IEEE Microwave and Wireless Components Letters*, vol. 29, no. 2, pp. 101-103, Feb. 2019.

[3] G. Shen, W. Che, W. Feng and Q. Xue, "High-Isolation Topology for Filtering Power Dividers Based on Complex Isolation Impedance and Surface Wave Suppression," *IEEE Transactions on Microwave Theory and Techniques*, vol. 69, no. 1, pp. 43-53, Jan. 2021.

[4] C. Han, D. Tang, Z. Deng, H. J. Qian and X. Luo, "Filtering Power Divider With Ultrawide Stopband and Wideband Low Radiation Loss Using Substrate Integrated Defected Ground Structure," *IEEE Microwave and Wireless Components Letters*, vol. 31, no. 2, pp. 113-116, Feb. 2021.

[5] J. -K. Xiao, X. -Y. Yang and X. -F. Li, "A 3.9GHz/63.6% FBW Multi-Mode Filtering Power Divider Using Self-Packaged SISL," *IEEE Transactions on Circuits and Systems II: Express Briefs*, vol. 68, no. 6, pp. 1842-1846, Jun. 2021.

[6] Y. -H. Zhu, J. Cai, Y. Cao and J. -X. Chen, "Compact Wideband Absorptive Filtering Power Divider With a Reused Composite T-Shape Network," *IEEE Transactions on Circuits and Systems II: Express Briefs*, vol. 70, no. 3, pp. 899-903, Mar. 2023.

[7] W. Feng, X. Ma, R. Gómez-García, Y. Shi, W. Che and Q. Xue, "Multi-Functional Balanced-to-Unbalanced Filtering Power Dividers With Extended Upper Stopband," *IEEE Transactions on Circuits and Systems II: Express Briefs*, vol. 66, no. 7, pp. 1154-1158, Jul. 2019.

[8] Z. Luo., "Dual-Band and Triple-Band Filtering Power Dividers Using Coupled Lines," *IEEE Transactions on Circuits and Systems II: Express Briefs*, vol. 70, no. 4, pp. 1440-1444, Apr. 2023.

[9] C. Bao, X. Wang, Z. Ma, C. -P. Chen and G. Lu, "An Optimization Algorithm in Ultrawideband Bandpass Wilkinson Power Divider for Controllable Equal-Ripple Level," *IEEE Microwave and Wireless Components Letters*, vol. 30, no. 9, pp. 861-864, Sept. 2020.

[10] N. Zhang, X. Wang, L. Zhu and G. Lu, "A Wideband Bandpass Power Divider With Out-of-Band Multi-Transmission Zeros and Controllable Equal-Ripple Levels," *IEEE Transactions on Microwave Theory and Techniques*, vol. 70, no. 2, pp. 1178-1187, Feb. 2022.

[11] H. Tian and Y. Dong, "Packaged Filtering Power Divider With High Selectivity, Extended Stopband and Wideband Isolation," *IEEE Transactions on Circuits and Systems II: Express Briefs*, vol. 70, no. 4, pp. 1311-1315, Apr. 2023.

[12] H. Tian, L. Xiao, H. Yu, Y. Chen, L. Shi and F. Xiao, "Wideband Microstrip Filtering Power Divider Designed by Direct Synthesis Technique (DST)," *IEEE Microwave and Wireless Components Letters*, vol. 32, no. 6, pp. 507-510, Jun. 2022.

[13] G. Zhang, Z. Qian, J. Yang and J. -S. Hong, "Wideband Four-Way Filtering Power Divider With Sharp Selectivity and High Isolation Using Coshared Multi-Mode Resonators," *IEEE Microwave and Wireless Components Letters*, vol. 29, no. 10, pp. 641-644, Oct. 2019.

[14] Park, Myun Joo, and B. Lee. "A symmetric coupled line equivalent circuit model for asymmetric coupled lines." *International Journal of RF and Microwave Computer-Aided Engineering*, vol. 26, no. 3, pp. 277-282, Apr. 2016.

[15] X. Wang, X. -W. Zhu, L. Tian, P. Liu, W. Hong and A. Zhu, "Design and Experiment of Filtering Power Divider Based on Shielded HMSIW/QMSIW Technology for 5G Wireless Applications," *IEEE Access*, vol. 7, pp. 72411-72419, 2019.

[16] X. Wang, J. Wang, G. Zhang, J. Hong and W. Wu, "Design of Out-of-Phase Filtering Power Divider Based on Slotline and Microstrip Resonator," *IEEE Transactions on Components, Packaging and Manufacturing Technology*, vol. 9, no. 6, pp. 1094-1102, Jun. 2019.

[17] B. -G. Liu, Y. -P. Lyu, L. Zhu and C. -H. Cheng, "Compact Square Substrate Integrated Waveguide Filtering Power Divider With Wideband Isolation," *IEEE Microwave and Wireless Components Letters*, vol. 31, no. 2, pp. 109-112, Feb. 2021.

[18] J. S. Hong and M. J. Lancaster, Microstrip Filters for RF/Microwave Applications. Hoboken, NJ, USA: Wiley, 2006

[19] D. Li, L. Zhang, J. Wang, Y. Liu and Q. Chen, "Characteristic Analysis Of Parallel And Anti-Parallel Coupled Line Structures And Their Integrated Design In Filtering Power Dividers," *IEEE Transactions on Components, Packaging and Manufacturing Technology*, Oct. 2023.

[20] K. Song, M. Fan, F. Zhang, Y. Zhu and Y. Fan, "Compact Triple-Band Power Divider Integrated Bandpass-Filtering Response Using Short-Circuited SIRs," *IEEE Transactions on Components, Packaging and Manufacturing Technology*, vol. 7, no. 7, pp. 1144-1150, Jul. 2017.

[21] X. Wang, Z. -C. Guo, J. Wang and L. Zhu, "Synthesis Design of a Self-Packaged Wideband Out-of-Phase Filtering Power Divider Implemented by PCB Lamination Process," *IEEE Transactions on Components, Packaging and Manufacturing Technology*, Oct. 2023.

[22] M. Danaeian, "A Novel Low Loss and Miniaturized Triple-Band Bandpass Filter and Equal/Unequal Filtering Power Dividers Using Half-Mode Substrate Integrated Waveguide," *IEEE Transactions on Components, Packaging and Manufacturing Technology*, vol. 13, no. 8, pp. 1254-1261, Aug. 2023 .

[23] C. Fan, X. Liu, Y. Liu, Y. Yang and Z. Zhu, "Wide-Stopband Substrate Integrated Waveguide Filter Power Divider Based on Through Glass Quartz Via (TQV) Technology," *IEEE Transactions on Components, Packaging and Manufacturing Technology*, vol. 12, no. 7, pp. 1196-1203, Jul. 2022.